Research Article

Optimization of the Desktop CPU's Straight Heatsink via CFD Simulation by Solidworks Flow Simulation

Md Nazmul Hasan Dipu[1, *], Mahbub Hasan Apu[2], Pritidipto Paul Chowdhury[1]

[1]Department of Industrial and Production Engineering, Shahjalal University of Science and Technology, Sylhet, Bangladesh.

[2]Department of Electrical and Electronic Engineering, Sylhet Engineering College, Sylhet, Bangladesh.

Article Info

Article history

Received: 06/12/2024
Revised 1: 13/01/2025
Accepted: 12/02/2025

Keywords:
Heatsink
CFD simulation
Thermal analysis
Forced convection
Heat transfer

ABSTRACT

The straight heatsink is one of the most common heat transfer components used in desktop CPUs to manage the heat generated by the microprocessor. The study aimed to find the optimal fin numbers of the straight heatsink for three different fin thicknesses and compare the masses at these points. For the analysis, the present study used Solidworks® software to create CAD models and perform the CFD simulation. It was found that each of the three different fin thicknesses had a turning point at which the microprocessor's temperature was at its minimum. The weight of the heatsink was also measured at those turning points. Specifically, the heatsinks with 1 millimeter, 1.5 millimeters, and 2 millimeters thickness had a microprocessor temperature of about 83.52 degrees Celsius, 86.50 degrees Celsius, and 89.25 degrees Celsius, with the weight of approximately 307.80 grams, 388.80 grams, and 448.2 grams. Overall, a 1-millimeter fin thickness with 21 fins configuration for this study was best under the criteria of minimum microprocessor temperature and minimum heatsink mass. Thus, this study successfully demonstrated that optimization of mass and fin thickness of the heatsink was possible to provide better thermal management of the microprocessors of a desktop's CPU. This study is significant for this era because it provides a panacea for minimum material cost, lightweight, and minimum microprocessor temperature.

1. Introduction

In this era, one of the most critical issues for electronic devices is the thermal management of their components [1]. Efficient thermal management is the cornerstone of high-performance computing, and the design of a CPU heatsink — spelled both ways: heatsink [2] and heat sink [3] — plays a pivotal role in maintaining system stability and longevity. Therefore, there are many significant reasons to incorporate an optimum heatsink for a desktop. Firstly, an optimum heatsink may prevent microprocessor failure because previously it was proven that thermal mismanagement was a major cause of the failure of the microprocessor [4]. Secondly, it offers faster clock speeds, which leads to better performance in smaller desktop designs [5]. Thirdly, it is indispensable for dispersing CPU heat and maintaining ideal operating temperatures [6].

Commonly, a heatsink is a device used to disperse heat from a component, such as a microprocessor, to improve thermal management [7]. Although there are many possible ways to design a heatsink by focusing on many criteria, the straight-fin heatsink is widely used [8] because they are simple, inexpensive, and robust. The physical structure of the heatsink usually has a segmented portion known as a fin — it improves heat dissipation by boosting the surface area [9] [10] [11]. The fins are mounted on a metal plate called the heatsink's base. This base generally needs to be attached to the microprocessor conductively. In order to increase the thermal conductivity, a thermal paste is usually used between the heatsink's base and the microprocessor. The typical arrangement [12] of a heatsink on a desktop is shown in ***Fig. 1***.

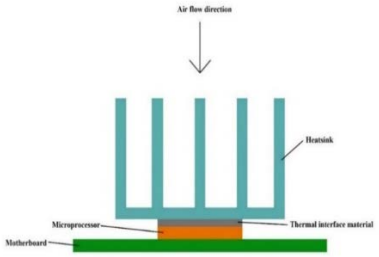

Fig. 1. A common attachment of microprocessor, heatsink, thermal interface material, and motherboard

For many years, the performance and optimization of straight-type heatsinks have been carried out [13] [14] [15]. For instance, Ozturk and Tari's research work utilized CFD (Computational Fluid Dynamics) software to analyze the temperature fields and flow of three CPU heatsink designs under coerced air-cooling conditions. The study considered fin shape, number of fins, materials, and base thickness for performance improvement. It was observed that the heatsink was improved by altering the shape and material, indicating these two were crucial factors [16]. Another study performed by Prabisha and Ramesh demonstrated that two new straight heatsink designs — straight

***Corresponding author:** Md Nazmul Hasan Dipu
*E-mail address: dipu.ipe.sust@gmail.com https://doi.org/10.56158/jpte.2025.113.4.01

corrugated and straight tapered — performed better than the conventional straight heatsink one [17]. On top of that, Hussain *et al.*'s study analyzed the impact of flow direction and fillet profile on the thermal performance of straight heatsinks. The study concluded that adding a fillet profile and changing flow direction improved heatsink performance [18]. Moreover, Kalbasi *et al.* conducted an experimental study on the Phase Change Material-based heatsinks and found that the optimal fin number of the heatsink decreased with the increment of the fin thickness [19]. Abdelmohimen *et al.* analyzed the impact of circular rods on heat transfer performance in a plate-fin heatsink. The study found that increasing rod number leads to decreased thermal resistance and increased pumping power. It was also mentioned that increased Reynolds and Nusselt numbers resulted in more cooling and higher pressure drop [20]. Additionally, Chiu *et al.* studied the heatsink numerically by Ansys with different arrangements of pin fins and found that the convergent-divergent arrangement had a lower effective thermal resistance than that with the staggered arrangement [21]. In support of this, Kosar and Peles's investigation [22] as well as Kosar *et al.* study [23] show that the efficiency of the micro heatsinks containing a staggered square pin-fin arrangement under the low-pressure drop had better results. One more experimental study carried out by Jassani on a vertical Aluminum heatsink with rectangular fins found that the reduction of spacing between two fins from 15 mm to 12 mm reduced the weight of the heatsink by 18%, while the heat transfer rate increased. As the length of the heatsink base was constant, lower spacing meant a higher number of fins [24]. It implies that a higher fin number of similar thickness increased heat transfer as well as reduced the mass of the heatsink.

Although literature studies were successful in addressing various aspects of heatsink optimization, there might be some existing research gaps, especially in heatsinks of desktop CPUs. Although the mass and fin thickness of the heatsink operating in desktop CPUs are important material cost factors, these might not have gotten proper attention in the earlier works. To address the aforementioned gaps, this study focused on several objectives. One objective was to find out the minimum mass of a straight heatsink in optimal situations. Another goal was to investigate the impact of fin thickness on heat-dissipating performance.

The rest of the structure of this article has three more sections. ***Section 2*** represents the methods of this simulation study. This section has six subsections: classical theory, CFD governing equations, CAD model, boundary conditions, Solidworks® flow simulation, and grid-independent test, sequentially. ***Section 3*** reveals the results of the analysis. Finally, ***Section 4*** illustrates the key findings, the significance of this study, and some limitations, blended with future directions.

2. Methods

2.1. Classical theory

Fin effectiveness is a dimensionless number because it is a ratio of a similar quantity. It is defined as the ratio of the actual heat transfer rate with fin(s) Q_{fin} to the heat transfer rate from the base area alone Q_{base} without any fin [25]. Q_{base} is the heat transfer rate from the base area as if no fins were present. The mathematical representation of fin(s) effectiveness is as follows [26] [27] [28]:

$$\text{Fin effectiveness, } \varepsilon = \frac{Q_{fin}}{Q_{base}} \quad (1)$$

$$\text{or, } Q_{fin} = \varepsilon \times Q_{base} \quad (2)$$

Fin efficiency η is another dimensionless quantity that measures a fin's performance by comparing its actual heat transfer rate Q_{fin} to the theoretical maximum heat transfer rate Q_{max} that could be attained if the entire fin(s) underwent the same temperature as its base. In other terms, Q_{ma} is the heat transfer rate if the entire fin were at the base temperature, which is not physically achievable but serves as a theoretical upper limit. Fin efficiency η measures how well the fin(s) uses its surface area to transmit heat. The mathematical representation of fin efficiency is as follows [27] [28] [29]:

$$\text{Fin efficiency, } \eta = \frac{Q_{fin}}{Q_{max}} \quad (3)$$

$$\text{or, } Q_{fin} = \eta \times Q_{max} \quad (4)$$

From the equations, the following relation can be obtained.

$$\varepsilon \times Q_{base} = \eta \times Q_{max} \quad (5)$$

$$\text{or, } \varepsilon = \eta \times \frac{Q_{max}}{Q_{base}} \quad (6)$$

Additionally, let the heatsink base area be A_{base} and the total surface of the fin(s) be A_{fin}.

$$Q_{max} = h\, A_{fin}\, \Delta T \quad (7)$$

$$\text{and, } Q_{base} = h\, A_{base}\, \Delta T \quad (8)$$

Here, h is the convective heat transfer coefficient. Again, ΔT is the same, because both experience the same temperature differences between base temperature and surrounding environment.

$$\varepsilon = \eta \times \frac{A_{fin}}{A_{base}} \quad (9)$$

Since the base of a heatsink is fixed, hence adding more fins increases the total fin surface area A_{fin} and thus the effectiveness ε is enhanced only if convection remains efficient. Conversely, if the aforementioned equation is formatted like the one below, it can be easily inferred that adding more fins increases the total surface area A_{fin}, but the efficiency η is exacerbated due to increased thermal resistance when convection becomes inefficient.

$$\eta = \varepsilon \times \frac{A_{base}}{A_{fin}} \quad (10)$$

Therefore, it can be assumed that until a certain fin number, an increment of the fin number leads to improved heat transfer; in contrast, after that certain fin number, fin efficiency will have deteriorated. From these classical theories, it is postulated that an optimal scenario exists. However, CFD simulation theories

are distinct; in the following subsection, CFD governing equations are described.

2.2. CFD Governing Equations

Generally, simulation software conducts the operations based on the following fundamental equations [30] [31]: continuity equation, momentum-conservation equations, and energy-conservation equations.

Continuity Equation [30]:

$$\frac{\partial(\rho u)}{\partial x}+\frac{\partial(\rho v)}{\partial y}+\frac{\partial(\rho w)}{\partial z}=0 \quad (11)$$

Here, u, v, and w represent velocities in the x, y, and z axes, whereas ρ represents fluid density.

Momentum-conservation equations [30] [32]:

In the x-direction:

$$\frac{\partial(\rho u)}{\partial t}+\frac{\partial(\rho uu)}{\partial x}+\frac{\partial(\rho uv)}{\partial y}+\frac{\partial(\rho uw)}{\partial z}=-\frac{\partial p}{\partial x}+\mu\left(\frac{\partial^2 u}{\partial x^2}+\frac{\partial^2 u}{\partial y^2}+\frac{\partial^2 u}{\partial z^2}\right)+\rho g_x \quad (12)$$

In the y-direction:

$$\frac{\partial(\rho v)}{\partial t}+\frac{\partial(\rho vu)}{\partial x}+\frac{\partial(\rho vv)}{\partial y}+\frac{\partial(\rho vw)}{\partial z}=-\frac{\partial p}{\partial y}+\mu\left(\frac{\partial^2 v}{\partial x^2}+\frac{\partial^2 v}{\partial y^2}+\frac{\partial^2 v}{\partial z^2}\right)+\rho g_y \quad (13)$$

In the z-direction:

$$\frac{\partial(\rho w)}{\partial t}+\frac{\partial(\rho wu)}{\partial x}+\frac{\partial(\rho wv)}{\partial y}+\frac{\partial(\rho ww)}{\partial z}=-\frac{\partial p}{\partial z}+\mu\left(\frac{\partial^2 w}{\partial x^2}+\frac{\partial^2 w}{\partial y^2}+\frac{\partial^2 w}{\partial z^2}\right)+\rho g_z \quad (14)$$

In these Navier-Stokes equations, μ represents dynamic viscosity, p represents static fluid pressure, t represents time, and g represents gravitational acceleration.

Energy-conservation equations [30]:

For the fluid:

$$\rho C_p\left(u\frac{\partial T_f}{\partial x}+v\frac{\partial T_f}{\partial y}+w\frac{\partial T_f}{\partial z}\right)=\lambda\left(\frac{\partial^2 T_f}{\partial x^2}+\frac{\partial^2 T_f}{\partial y^2}+\frac{\partial^2 T_f}{\partial z^2}\right) \quad (15)$$

Where T_f is the fluid temperature, λ is the thermal conductivity, and C_p is the fluid's specific heat capacity.

For the solid:

$$k\left(\frac{\partial^2 T_s}{\partial x^2}+\frac{\partial^2 T_s}{\partial y^2}+\frac{\partial^2 T_s}{\partial z^2}\right)=0 \quad (16)$$

Where k and T_s are the thermal conductivity and temperature of the solid, accordingly.

It is difficult to calculate the result manually using these equations. Therefore, commercial CFD simulation software — Solidworks® 2023 — was employed in this study to calculate the outcomes. Albeit the CFD method requires much time to perform an analysis, its result is highly accurate for thermal analysis, despite the complex geometry of the model [33]. Moreover, in CFD, more complex factors can be incorporated, such as conjugated heat transfer.

2.3. CAD model and components' materials

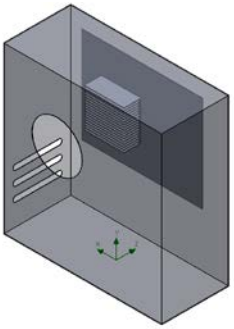

Fig. 2. Assembled model in Solidworks® 2023

All Solidworks® 2023 part files — a straight heatsink, a casing, a PCB as a common motherboard, a microprocessor, and thermal interface material — were assembled as in *Fig. 2*. Attachment of motherboard, microprocessor, thermal interface material, and heatsink was followed by an earlier mention in *Fig. 1*.

Firstly, the part case had an overall dimension of 400×170×420 cubic millimeters and a 170-millimeter diameter hole for the inlet cooling fan boundary condition purpose. Moreover, it had three air vent holes on the rear surface to exhaust the airflow. The casing hull thickness was 1 millimeter. The casing material was mild steel. Secondly, the motherboard had an overall dimension of 304.8×243.84×1.5 cubic millimeters. Thirdly, the microprocessor size was considered to be 37.5×37.5×5 cubic millimeters to mimic the *Intel i9 9900k* microprocessor's lid size [34]. Its material was copper. In this present work, the microprocessor engendered 100 watts of heat during simulation analysis. The dimension of the heatsink was considered, as earlier mentioned. Fourthly, the thickness of the thermal interface material was considered to be 0.1mm between the heatsink base and the microprocessor. Its length and width were the same as those of the microprocessor. Finally, the heatsink had dimensions according to the boundary conditions of the present study.

2.4. Boundary conditions and necessary assumptions

To run the CFD simulation, some boundary conditions and necessary assumptions are required [35] in light of the objective of the study. In this present study, all the following boundary conditions and assumptions were made to execute the Solidworks® Flow Simulation.

a) The fin was subjected to forced convection heat transfer. Forced convection, unlike natural convection, uses a mechanical device, such as a fan or pump, to compel the fluid to flow through the target surface [36]. Natural convection-based cooling is called passive cooling, while forced convection-based cooling is known as active cooling [37]. Thus, heatsinks that depend on natural convection are called passive heatsinks [38]. On the other hand, active heatsinks rely on forced convection [38].
b) Ramakrishnan *et al.* wrote that the Intel i9 9900k had a thermal design power of 95 watts [34]. Additionally, while the average Thermal Design Power (TDP) is 95 watts for *Intel i9 9900k* [39], it never really crosses the 100 watts

limit [40]. Therefore, in this study, it was assumed that the CPU's microprocessor generated constant heat power, which was 100 watts.

c) Standard ambient temperature was taken for the environment's air as a 25-degree Celsius temperature [41] [42] [43], and atmospheric pressure was considered to be exactly 101325 Pascal pressure [44] [45].

d) The fan was internally mounted (inside the casing), and it was a *"JMC 7015-12H axial product"*. It was a predefined fan in Solidworks® 2023 software. It was chosen from the "conditions command manager," which is why it is not shown in the assembled CAD model.

e) Materials for the casing, heatsink, microprocessor, thermal interface material (thermal paste), and motherboard were mild steel, aluminum 6061, copper, GR25A, and PCB 4-layers from the Solidworks® 2023 standard material library (pre-defined materials). Here, aluminum 6061 was chosen for this study's heatsink because the aluminum 6061 properties, i.e., low weight, high strength, ease of processing, low-temperature resistance, corrosion resistance, and low maintenance, are all advantages [46] [47]. In addition, the GR25A Series is an extremely malleable and thermally conductive gel substance [48].

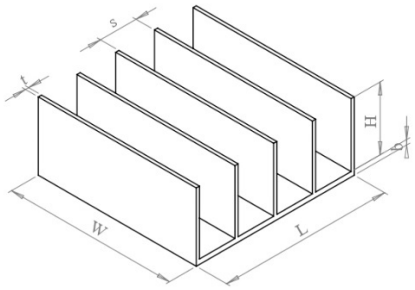

Fig. 3. Straight heatsink geometrical parameters

f) *Fig. 3* shows the straight heatsink geometrical parameters. In this present study, length (L), width (W), height (H), and base thickness (b) were constant, and they were 100, 100, 40, and 3 millimeters, respectively. Howbeit, each fin thickness varied — 1, 1.5, and 2 millimeters — in order to perform the analysis, as did the space between two fins, and the number of total fins also varied. When the number of fins varied from 2 to 40 for a particular heatsink, the space between the two fins changed, respectively.

g) Based on solid boundaries, there are two types of flow analyses: internal flow analysis and external flow analysis. Internal flow analysis examines fluid movement between solid surfaces, such as tanks. Internal flows are contained within geometry. Oppositely, in external flow analysis, fluid flow is not limited by an outside physical surface, but rather by the bounds of the Computational Domain. A *lid* is not necessary unless the application incorporates a flow source, such as a fan. This current analysis was performed under the boundary condition of external flow. Because not only did the cooling fan allow contact with room temperature and pressure between ambient fluid and casing inside the fluid, but also three air vents did.

h) Instead of auto mesh, a manual mesh was chosen — 20 values for each number of cells per X, Y, and Z — for all configurations analyses when the heatsink was modified for thicknesses and fin numbers. A specific mesh was useful to maintain consistency for analysis, which led to better results. After each modification in the 3D model for variation data pertinent to different fin numbers, re-meshing is necessary.

i) Computational domain is a crucial step in Computational Fluid Dynamics [49]. The computational domain is an external volumetric region that surrounds the model and is used to discretize and solve the basic flow equations. A typical domain has six boundaries that define its circumstances. These are mostly non-physical boundaries. Non-physical boundaries should be placed far enough away from the model to avoid significant influences on the results and to keep the results accurate [50]. In this present simulation study, the computational domain was considered to have constant dimensions — default values — throughout the entire study, so the comparison of the results was logical.

j) A total of four lids — a Solidworks® 2023 tool, namely "*Creating Lids*," which is a mandatory requirement in Solidworks® 2023 to perform flow simulation analysis where the electronics enclosure has at least one cutout hole — were created. One of them was used to apply the inlet fan boundary condition, and the other three were used to apply fluid exhaust. Furthermore, it needs to be clarified that lids are not normally employed in natural convection situations. However, the present study was conducted via coerced convection; hence, lids could be used.

2.5. Solidworks® Flow Simulation

In this study, a total of 117 (39 for each fin thickness) data points were generated by *Solidworks® Flow Simulation* — a CFD tool. To help readers understand this article, a detailed description of how these data were created by CFD simulation is needed. But instead of describing all 117 data points, one datum is explained because the rest of the others follow the same steps after altering the desired fin thicknesses and fin numbers properly. Here is a step-by-step process for performing a CFD thermal analysis of a heatsink — for the 1-millimeter fin thickness and 2 number of fins — using *Solidworks® Flow Simulation*:

Firstly, for the first time use, it was mandatory to enable the *Solidworks® Flow Simulation* add-in. Thus, from the standard toolbar, it was required to go to Tools > Add-Ins, and *Solidworks® Flow Simulation* was activated. This led to the visible Flow Simulation tab.

Secondly, opening the assembled CAD model was required which was created based on the relevant dimensions and components mentioned above.

Thirdly, from the *Flow Simulation* tab, *Create New Simulation Project* was clicked. At that moment, both the *Computational Domain* and *Mesh Settings* were reset. Necessary *Lids* were created to make the model watertight.

Fourthly, a *Wizard* was clicked where a *Create New* configuration was chosen right the first time for this project. From the new pop-up window, the *SI* unit system was selected

except for temperature in degrees Celsius. Moreover, *Fluid Flow*, *Conduction*, and *Gravity* were marked. The gravity direction was corrected downward according to the model if needed. For this present study, the reverse Y direction was used. In other words, the gravity value was -9.81 meters per second square. However, the *Rotation* box was not marked, although a fan was used in this study. The reason behind this is that the fan used in this study was incorporated from the Solidworks® *Pre-defined* fan library as a boundary condition via selecting the target *lid* face, described in the later step in this article, for making the analysis with the market standard fan. In other words, there was no physical model of the fan or its blades in the study; only the Solidworks® engineering fan database was used. Moreover, *Conduction* was marked because heat was supposed to be transferred from the microprocessor to the heatsink by conduction. Additionally, from the same window, the *External* analysis type was chosen. *Geometry Recognition* was *CAD Boolean*, and the cavity was excluded without conditions like default. Additionally, only *Air* was added as a fluid from the *Gases* list. The *flow type* was kept *Laminar and Turbulent* as the default. Furthermore, a default solid material in the wizard was assertively needed, and the *EPS Slab* was chosen as a placeholder material. Ironically, the correct materials for each component individually were assigned later. Thus, there was no impact from it. In addition, the wall *Roughness* was 0 *micrometers*. Besides, the *Coordinate System* was in the *Z* direction because the cooler fan was supposed to flow the air in this direction for this study's CAD model — the fan's cutout hole exists in this direction.

Fifthly, the corresponding *Solid Material* was employed for each component from the *Sources* command manager. In this study's model, the desktop casing was composed of mild steel, while the heatsink was supposed to be made of aluminum. The printed circuit board (PCB), representing the motherboard, consisted of a four-layer PCB material. Copper material was selected for the microprocessor, and the thermal interface material was *Fujipoly GR25A*.

Sixthly, the *Boundary Condition* was chosen by the *Condition* command manager for three air-bent lids where the *Type* was *Pressure Opening* as *Environment Pressure*. In addition, *Thermodynamic Parameters* were 101325Pa and 25°C. The coordinating system was global, and the reference axis was *X* by default.

Seventhly, it was time to choose a fan for the desktop cooling fan. To utilize a fan as a boundary condition, the *Fan* was clicked from the *Condition* command manager. There are three fan *Types*: *External Inlet Fan*, *External Outlet Fan*, and *Inlet Fan*. An *External Inlet Fan* supplies air or fluid into the system from the external environment. It is usually located outside the enclosure or system. On the contrary, an *External Outlet Fan* removes air or fluid from the system into the external environment. Lastly, the *Inlet Fan* located within the system introduces flow directly into the domain. This kind of fan is an integral part of the device, like HVAC ducts or cooling fans in electronics. Alternatively, the *Inlet Fan* is an internal component of the system that is mounted inside the enclosure. For this present study, an *Inlet Fan* namely a *JMC 7015-12H axial product* was picked from the *Pre-Defined* fan list. Because a CPU fan is located inside the desktop case, and its purpose is to direct airflow over the CPU heatsink to dissipate heat. This makes it an integral part of the internal system rather than an external boundary. Moreover, the fan introduces airflow directly into the domain (i.e., over the CPU heatsink), making the *Inlet Fan* type the most appropriate for simulating this behavior. For this present study, "*Faces fluid exits the fan"* was the fan *Lid*, and "*faces fluid enters the fan" was the* casing, the outer face where a cutout hole was available. The coordinating system was the *face coordinate system*, and the reference axis was Z for both. Parameters such as *Thermodynamic* and *Turbulent* were marked.

Eighthly, from the *Sources* command manager, *Volume Source* was clicked, followed by 100 watts *Heat Generation Rate* was chosen as the *Heat Source* for the microprocessor. Here, the coordinating system was global, and the reference axis was X by default.

Ninthly, *Volume Goal* was picked from the drop-down menu of *Goals.* The microprocessor was chosen to determine its maximum *Temperature (Solid)* value. The *convergence control* was marked by default. In addition, the *Global Goals* were chosen for determining the *Heat transfer Coefficient*, and only the *Average* box was marked.

Tenthly, *Global Mesh* was selected from the *Mesh* command manager. The *Basic Mesh* value was manually input as 20 for all directions to keep the analysis consistent. Further, the *number of cells across the channel* was 5, and the maximum refinement value was 2.

Finally, the simulation study was Run, and obtained maximum microprocessor temperature obtained from the *Solver's Goal Plot* was recorded in the corresponding MS Excel sheets. In this case, — for the 1-millimeter fin thickness and 2 number of fins — the maximum microprocessor temperature was 185.08 degrees Celsius, and it was stored in Table ***2*** in the first-row. Also, the average heat transfer coefficient was about 2.83$W.m^{-2}.k$ which was obtained from the *Solver's Goal Plot* and it was recorded in Table ***5***. These tables are available in this article under ***Section 3***: Results and discussion.

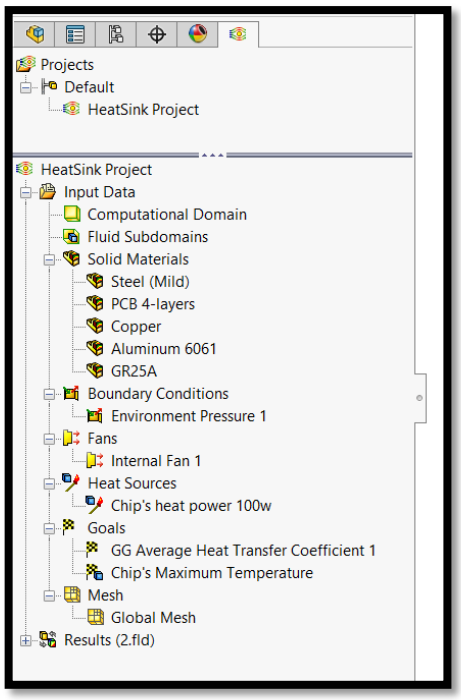

Fig. 4. Appearance of the Feature Manager after applying boundary conditions and assumptions

For the rest of the data, the aforementioned settings were kept the same, and there was no alteration in the *Flow Simulation Analysis* in *Feature Manager*. To say alternatively, *Feature Manager* was kept like ***Fig. 4*** for the rest of the data. However, desired fin numbers and fin thickness were alerted prior to each *Run.* Eventually, Table ***2***, Table ***3***, and Table ***4*** were prepared for the 1-millimeter fin thickness, 1.5-millimeter fin thickness, and 2-millimeter fin thickness, respectively. These tables are also available in the results and discussion ***Section 3***. Each of these tables has 39 data points for discrete fin numbers from 2 to 40. To help the readers easily understand the process flow for all 117 data points, a flowchart ***Fig. 5*** has been provided.

2.6. Grid Independent Test

A larger number of elements or cells produces a more accurate output; nevertheless, simulating a larger number of elements takes a longer time [35]. Natheless, it is also essential to ensure that the accuracy of the result is acceptable. In this simulation, the grid-independent test was conducted for the 1-millimeter fin thickness with a fin number of 2. To perform the grid-independent test, the *number of cells across the channel* in the *global mesh* was altered from 4 to 5, then from 5 to 6. This modification led to a change in the total cell number in the solver's information. For these varying total cell numbers, different microprocessor maximum temperature was achieved, as shown in Table ***1***. Therefore, a comparison of the obtained microprocessor maximum temperature could be made. Comparing the *number of cells across the channel*, particularly one before and one after, shows that 5 *number of cells across the channel* were good enough for this present study. Because it had an acceptable small percentile of maximum temperature differences. It indicated that the influence of the mesh size on the result was acceptable and tolerable. Thus, 5 *number of cells across the channel* were carried out in the description under ***subsection 2.5*** in this article.

Table 1. Grid independent test for a specific heatsink

Number of cells across the channel	***Total cells***	***Microprocessor maximum temperature for a certain heatsink (degrees Celsius)***	***Temperature difference (percentage)***
One before the used value for the study = 4	16678	190.28	
The value used for this study = 5	18421	185.08	- 2.80 %
One after the used value for the study = 6	20991	181.44	- 2.00 %

3. Results and discussion

To begin with, the 1-millimeter fin thickness, the number of fins was increased from 2 to 40 to examine the influence of the fin numbers on the microprocessor's temperature. It was noticed that the microprocessor's temperature was continuously shrunk until the fin number reached 19. However, some fluctuations were witnessed in fin number 20 to fin number 40. Among these fluctuations, the lowest temperature — nearly 83.52 degrees Celsius — was detected for 21 fins for the 1-millimeter fin thickness. The lowest temperature for the simulation analysis of the 1-millimeter fin thickness is referred to as the Global Minimum temperature; other convex points are called the Local Minimum [51]. Table ***2*** depicts the simulation test results for the 1-millimeter fin thickness from the fin numbers 2 to 40, where the corresponding temperature and comment are mentioned for each fin number.

.

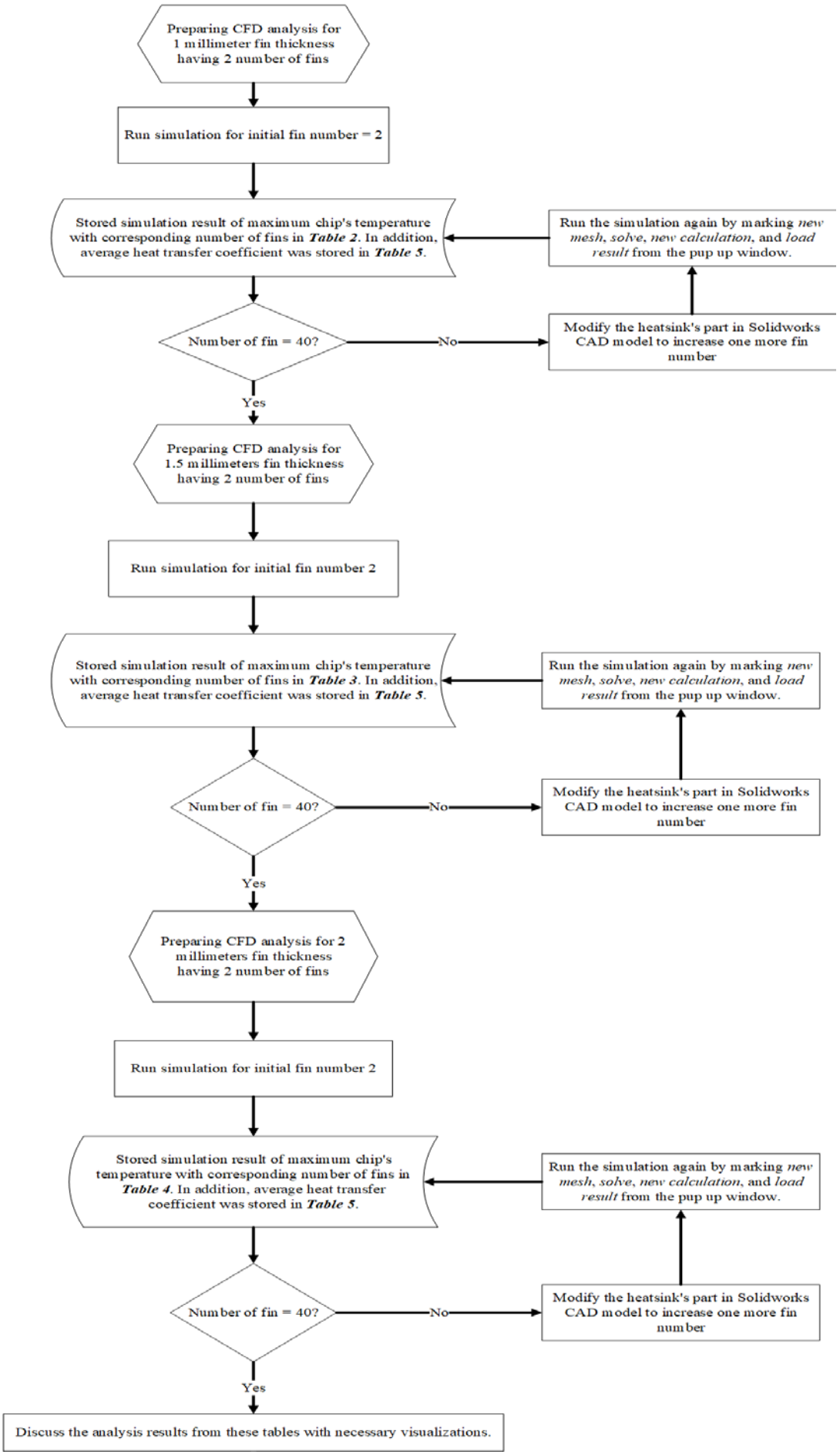

Fig. 5. A flowchart about the conduct of simulation studies for 117 distinct heatsink configurations

Table 2. Maximum microprocessor temperature values for various fin numbers while fin thickness remained constant at 1 millimeter

Fin thickness (millimeter)	Number of fins	Maximum microprocessor temperature (°C)	Comment for maximum microprocessor temperature
1	2	185.08	---
1	3	167.86	decreasing
1	4	157.02	decreasing
1	5	146.27	decreasing
1	6	140.83	decreasing
1	7	135.52	decreasing
1	8	128.30	decreasing
1	9	120.96	decreasing
1	10	116.93	decreasing
1	11	110.74	decreasing
1	12	106.65	decreasing
1	13	102.14	decreasing
1	14	99.21	decreasing
1	15	95.48	decreasing
1	16	92.29	decreasing
1	17	88.98	decreasing
1	18	87.84	decreasing
1	19	85.42	decreasing (Local Minimum)
1	20	85.48	increasing, (Local Maximum)
1	**21**	**83.52**	**decreasing, (Global Minimum)**
1	22	84.00	increasing
1	23	84.06	increasing, (Local Maximum)
1	24	83.72	decreasing, (Local Minimum)
1	25	85.96	increasing, (Local Maximum)
1	26	85.94	decreasing, (Local Minimum)
1	27	86.18	increasing
1	28	86.76	increasing
1	29	87.32	increasing
1	30	87.35	increasing
1	31	89.27	increasing, (Local Maximum)
1	32	88.92	decreasing, (Local Minimum)
1	33	91.07	increasing
1	34	92.26	increasing
1	35	92.61	increasing
1	36	93.39	increasing
1	37	93.51	increasing
1	38	95.81	increasing, (Local Maximum)
1	39	95.46	decreasing, (Local Minimum)
1	40	97.13	increasing

Another fin thickness for this study was 1.5 millimeters. Like the aforementioned simulation test, the number of fins was also increased from 2 to 40 to examine the impact of the fin numbers on the microprocessor's temperature by this thickness. During the analysis, it was discerned that the microprocessor's temperature was gradually lessened from the commencement until the fin number arrived at 19. Subsequently, there were some oscillations in the microprocessor's temperature with respect to the fin number between 20 and 24. On the contrary, the temperature of the microprocessor consistently climbed during the fin number from 25 to 40. Among all of the turning points, the Global Minimum temperature was approximately 86.50 degrees Celsius when the fin number was 19. Table ***3*** demonstrates the iterations for the fin thickness of 1.5 millimeters from fin number 2 to 40. This table also provides the record of the microprocessor's temperature corresponding to each fin number period to the analysis.

Table 3. Maximum microprocessor temperature values for various fin numbers while fin thickness remained constant at 1.5 millimeters

Fin thickness (millimeter)	Number of fins	Maximum microprocessor temperature (°C)	Comment for maximum microprocessor temperature
1.5	2	183.05	---
1.5	3	167.36	decreasing
1.5	4	156.38	decreasing
1.5	5	146.06	decreasing
1.5	6	141.03	decreasing
1.5	7	134.71	decreasing
1.5	8	127.06	decreasing
1.5	9	119.84	decreasing
1.5	10	115.39	decreasing
1.5	11	109.72	decreasing
1.5	12	105.28	decreasing
1.5	13	100.83	decreasing
1.5	14	96.77	decreasing
1.5	15	93.45	decreasing
1.5	16	91.21	decreasing
1.5	17	88.37	decreasing
1.5	18	86.61	decreasing
1.5	**19**	**86.50**	**decreasing, (Global Minimum)**
1.5	20	87.89	increasing, (Local Maximum)
1.5	21	87.04	decreasing, (Local Minimum)
1.5	22	88.41	Increasing
1.5	23	89.34	increasing, (Local Maximum)
1.5	24	87.77	decreasing, (Local Minimum)
1.5	25	90.93	increasing
1.5	26	91.26	increasing
1.5	27	93.82	increasing
1.5	28	94.10	increasing
1.5	29	94.78	increasing
1.5	30	97.21	increasing
1.5	31	98.63	increasing
1.5	32	100.33	increasing
1.5	33	101.77	increasing
1.5	34	103.53	increasing
1.5	35	105.77	increasing
1.5	36	107.28	increasing
1.5	37	108.32	increasing
1.5	38	110.96	increasing
1.5	39	113.02	increasing
1.5	40	114.96	increasing

One more fin thickness for this study was 2 millimeters. Fin numbers of this heatsink also underwent escalation from 2 to 40. During the investigation, it was discovered that the microprocessor's temperature progressively decreased from the beginning until the fin number reached 17. Followed by the expansion of the temperature and obtained a concave point at fin number 20; however, it had a convex point immediately at fin number 21. For the fin number from 22 to 35, it endured temperature growth. Notwithstanding, it had undergone some concave and convex points for the rest of the fin numbers. Among all the convex points that the 2-millimeter fin thickness heatsink had in this study, the Global Minimum was achieved at fin number 17, for which the microprocessor temperature was around 89.35 degrees Celsius. Table ***4*** shows all records pertinent to the simulation study for this 2-millimeter fin-thickness heatsink.

Table 4. Maximum microprocessor temperature values for various fin numbers while the fin thickness remained constant at 2 millimeters

Fin thickness (millimeter)	Number of fins	Maximum microprocessor temperature (°C)	Comment for maximum microprocessor temperature
2	2	183.39	---
2	3	165.97	decreasing
2	4	154.72	decreasing
2	5	145.21	decreasing
2	6	140.93	decreasing
2	7	131.67	decreasing
2	8	126.56	decreasing
2	9	118.65	decreasing
2	10	114.15	decreasing
2	11	108.98	decreasing
2	12	103.96	decreasing
2	13	98.52	decreasing
2	14	95.41	decreasing
2	15	92.01	decreasing
2	16	91.50	decreasing
2	**17**	**89.25**	**decreasing, (Global Minimum)**
2	18	90.40	increasing
2	19	90.73	increasing
2	20	92.82	increasing, (Local Maximum)
2	21	91.48	decreasing, (Local Minimum)
2	22	94.46	increasing
2	23	96.63	increasing
2	24	97.21	increasing
2	25	99.60	increasing
2	26	101.56	increasing
2	27	103.70	increasing
2	28	106.09	increasing
2	29	108.02	increasing
2	30	111.30	increasing
2	31	113.64	increasing
2	32	114.65	increasing
2	33	114.73	increasing
2	34	118.18	increasing
2	35	119.39	increasing, (Local Maximum)
2	36	119.04	decreasing, (Local Minimum)
2	37	120.80	increasing
2	38	122.07	increasing, (Local Maximum)
2	39	119.50	decreasing, (Local Minimum)
2	40	124.35	increasing

A total of 117 simulation analyses were executed, with 39 simulation analyses for each of the three variations of fin thicknesses — 1-millimeter fin thickness, 1.5-millimeter fin thickness, and 2-millimeter fin thickness — from fin number 2 to fin number 40. The microprocessor's maximum temperature was recorded each time for the respective fin number in Table ***2***, Table ***3***, and Table ***4*** for the fin thicknesses 1 millimeter, 1.5 millimeter, and 2-millimeter, respectively. These temperature and fin number data have been visually presented in ***Figs. 6a–c***. From the graphs, it is evident that the heatsink had a Global Minimum point (critical turning point) for each of the three different fin thicknesses. The Global Minimum temperatures for 1-millimeter fin thickness, 1.5-millimeter fin thickness, and 2-millimeter fin thickness were about 83.52 degrees Celsius, 86.50 degrees Celsius, and 89.35 degrees Celsius, respectively, and corresponding fin numbers were 21, 19, and 17, depicted in ***Fig. 6a, Fig. 6b,*** and ***Fig. 6c*** in order.

Before the Global Minimum turning point in all three graphs, why did the temperature of the microprocessor fall almost gradually with the fin number increment in ***Figs. 6a–c***? The reason behind it was the surface area. The increment of the fin numbers, for instance, from fin number 2 to fin number 3, leads to the enlargement of the heatsink surface area. This increased surface area could dissipate more heat. Thus, the temperature decreased almost continuously with the increment in fin number prior to the Global Minimum.

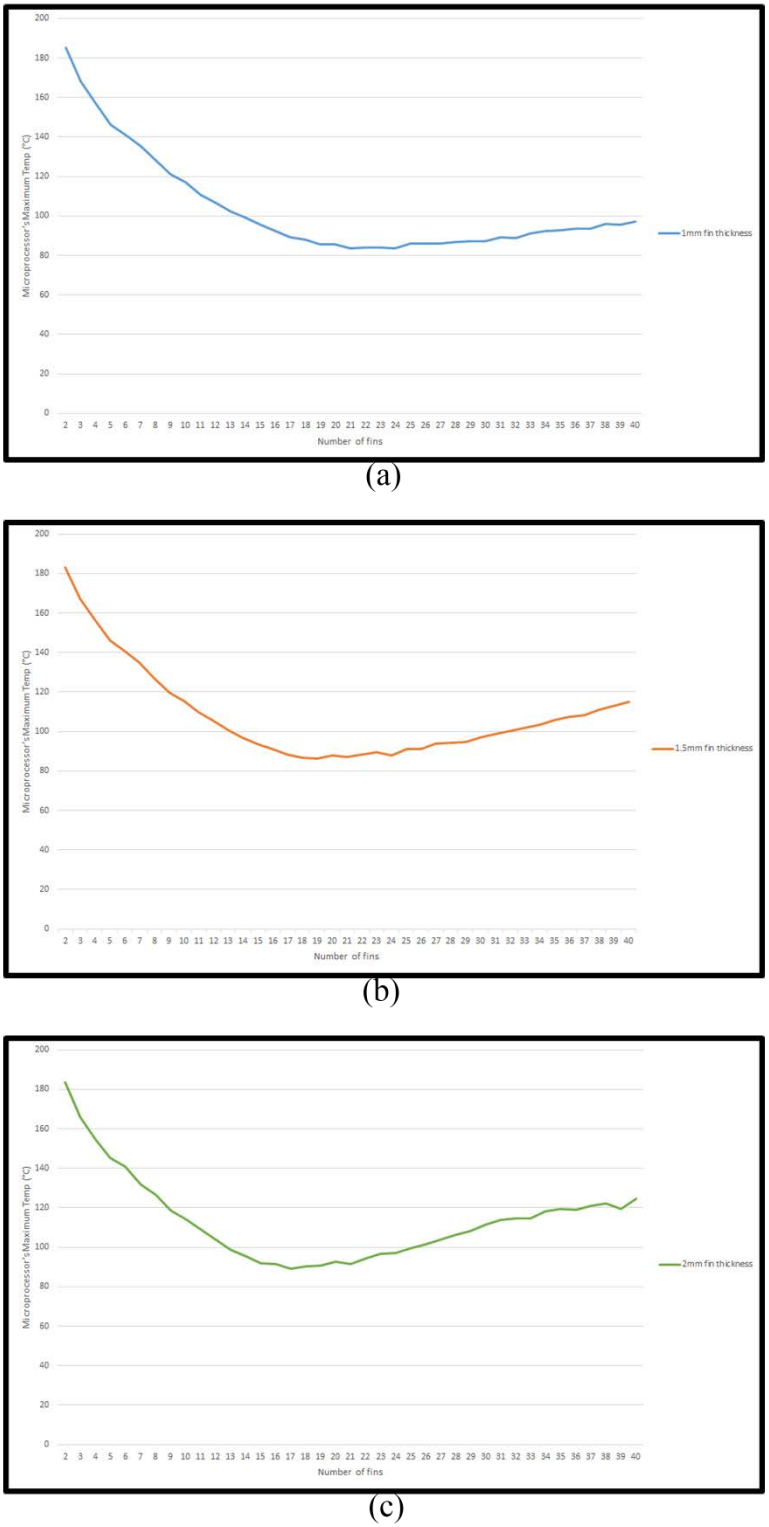

Fig. 6. Microprocessor's maximum temperature vs. number of fins for three different fin thicknesses

However, the graphs following the Global Minimum turning points, why did the temperature of the microprocessor rose fairly smoothly as the fin number increased in ***Figs. 6a–c***? The cause was the limited room for airflow. Though the surface area was increased with respect to the fin number growth like in the earlier scenario, room for smooth airflow continuously deteriorated. Because each time the newly incremented fin took a certain amount of space, which curtailed the free space for airflow. As a consequence, less heat was transferred by the heatsink. Therefore, microprocessor temperature was almost gradually inflated for the increment of fin number after the Global Minimum point. In addition, have you noticed that the graph of 2-millimeter fin thickness is the sloppiest while the graph of 1-millimeter fin thickness is the least sloppy, afterward the Global Minimum turning point? Every scientific phenomenon has a reason behind it. In this case, nonetheless, fin thicknesses are varied; length, width, and height are constants for the heatsink. Therefore, for the same fin numbers but varying thicknesses, the heatsink of the thin fin could provide better airflow than that of the thick fin. As a result, the temperature of the thin fin is less than that of the thick fin heatsink.

Table 5. Average heat transfer coefficient for different fin configurations

Number of fins	*Heat transfer coefficient*		
	1-millimeter fin thickness ($W.m^{-2}.k$)	*1.5-millimeter fin thickness ($W.m^{-2}.k$)*	*2-millimeter fin thickness ($W.m^{-2}.k$)*
2	2.83	2.51	2.88
3	2.78	2.78	2.71
4	2.64	2.62	2.72
5	2.69	2.91	2.64
6	2.71	2.65	2.63
7	2.70	2.72	2.76
8	2.72	2.72	2.71
9	2.77	2.76	2.78
10	2.83	2.85	2.84
11	3.04	2.93	2.96
12	3.01	3.02	3.04
13	3.10	3.06	3.16
14	3.12	3.18	3.18
15	3.23	3.26	3.29
16	3.30	3.31	3.26
17	3.39	3.48	3.29
18	3.47	3.45	3.25
19	3.52	3.41	3.48
20	3.55	3.31	3.09
21	3.56	3.56	3.10
22	3.53	3.62	2.96
23	3.50	3.20	3.17
24	3.50	3.38	3.20
25	3.52	3.31	3.06
26	3.60	3.04	3.00
27	3.39	3.22	2.98
28	3.32	3.19	2.95
29	3.44	3.03	2.87
30	3.14	3.03	2.77
31	3.36	3.06	2.78
32	3.35	3.04	2.66
33	3.31	2.92	2.72
34	3.19	2.87	2.66
35	3.15	2.86	2.65
36	3.20	2.80	2.68
37	3.09	2.84	2.63
38	2.92	2.73	2.62
39	2.87	2.67	2.60
40	2.87	2.69	2.62

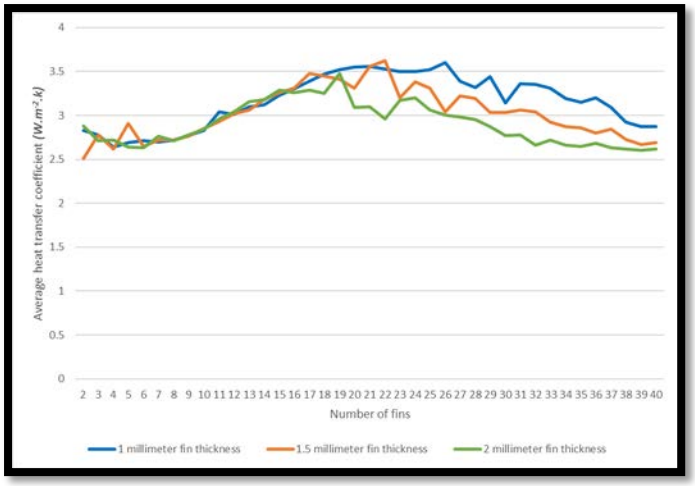

Fig. 7. Average heat transfer coefficient vs number of fins for different heatsink configurations

The average heat transfer coefficient was also monitored for the different heatsink configurations and the corresponding data were recorded in Table ***5***. Based on Table ***5***, a plot was generated to depict the three-line graphs for all three diverse fin thicknesses, shown in ***Fig. 7***. In the direction of the X-axis, the number of fins was placed; on the other hand, the average heat transfer coefficient was put toward the Y-axis. These three graphs seem to be almost concave because, in the middle portions, they have the optimal fin numbers for each corresponding fin thickness configuration. For those optimal fin numbers, the average heat transfer coefficient is slightly higher in the three graphs in the middle portions. In addition, from the commencing until fin number 15 for three fin thicknesses, they witnessed almost closed average heat transfer coefficient values. The reason behind this might be the room for air-flow space was very sufficient for all three kinds of thicknesses. But after that,

the comparatively thicker fin thickness heatsinks spoiled the space rapidly leading to the separation of three-line graphs.

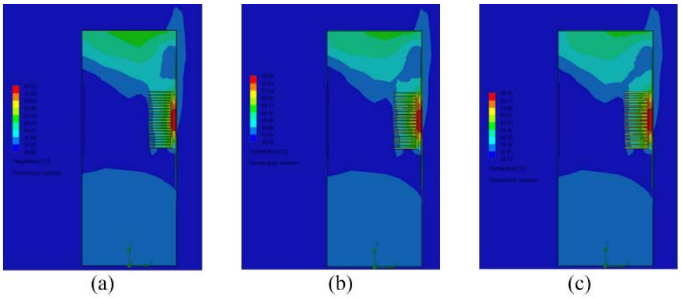

Fig. 8. Temperature contours at the heatsink's midplane when the microprocessor reached a Global Minimum temperature

As ***Figs. 6a–c*** demonstrates that the heatsink had a Global Minimum point for each of the three different fin thicknesses. Hence, three temperature *cut-plots* were created— shown in ***Figs. 8a–c*** — at the midplane of the heatsink in order to show the temperature contours — it is a useful and effective graphic technique to view some sorts of CFD results [52]. ***Fig 8a*** represents the temperature contour for 1-millimeter fin thickness at the Global Minimum point — the fin number 21. Analogously, ***Fig 8b*** and ***Fig 8c*** illustrate the temperature contour for 1.5-millimeter fin thickness and 2-millimeter fin thickness at the corresponding Global Minimum points — the fin numbers 19 and 17, respectively. These temperature contours help to understand what would happen if it were in real circumstances. Here, extreme indigo portions indicate the room temperature air, which was coerced from the left to the right by a cooling fan directed at the heatsink. It is because room-temperature air would have the lowest temperature. On the other hand, red portions — the microprocessor unit — demonstrate the maximum temperature. The air surrounding the microprocessor is supposed to have the highest temperature air by nature, as it is the main heat source. A green portion can be seen at the top of the casing because comparatively hot air tended to go upward. A light blue portion can be seen at the bottom of the casing because this air was supposed to go out from the casing to the ambient air via three back air vents. Thus, these simulations replicate the natural phenomenon, indicating the credibility of the study's settings in the CFD software.

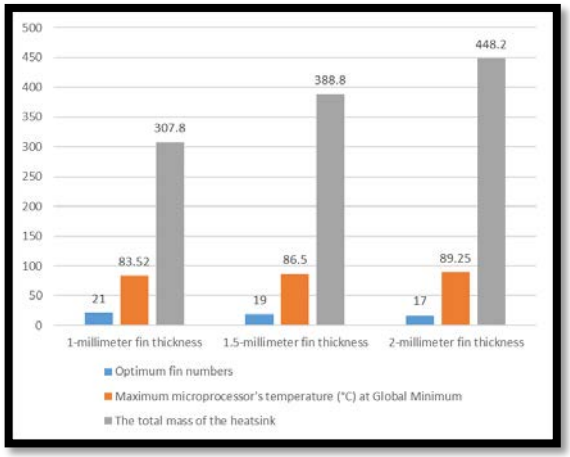

Fig. 9. A clustered bar chart of three different fin thicknesses when they got the optimal situation

A comparison of heatsinks with three different fin thicknesses could be performed in terms of Global Minimum microprocessor temperatures and mass. The mass can be found in the 3D models by the Solidworks® feature after applying the material to the objects. In order to compare the data visually, first, it is essential to keep the desired comparable data in a table. Thus, Table ***6*** was prepared to put the Global Minimum data. Those data, such as fin thicknesses, microprocessor temperatures, and masses, were stored in Table ***6*** corresponding to the Global Minimum points' fin numbers. Thereafter, a clustered bar chart ***Fig. 9*** was produced by MS Excel based on Table ***6*** in order to compare all three Global Minimum situations. This clustered bar chart displays that a heatsink whose fin thickness was 1 millimeter has not only the lowest minimum temperature but also the lowest weight compared to the other two heatsinks. Albeit this 1-millimeter fin had more fin numbers compared to others, the cost of material and performance of the heatsink got more priority. Therefore, it is unraveled from the comparison that 1-millimeter fin thickness had not only the most heat transfer performance but also the least weight among all three sorts of fin thicknesses.

Table 6. Properties of the heatsinks at the three mentioned Global Minimum points

Properties	Fin thickness 1 millimeter	Fin thickness 1.5 millimeters	Fin thickness 2 millimeters
Optimum number of fins	21	19	17
Microprocessor's temperature (°C) at a Global Minimum	83.52	86.50	89.25
The total mass of the heatsink (grams)	307.8	388.8	448.2

4. Conclusion, limitations, and future works

4.1. Conclusion

This research focused on mitigating the weight of a straight heatsink in optimal situations and investigated the influence of fin thickness on thermal management in microprocessors. The CFD simulation study demonstrated several insights, which are mentioned below:

- ✓ The CFD simulation study demonstrated that less fin thickness (at Global Minimum points for all three thicknesses) leads to both less heatsink weight and a minimum temperature of the microprocessor. For this present study, the optimal fin thickness was found to be 1 millimeter. The Global Minimum point for this 1-millimeter fin thickness type heatsink was at fin number 21. For this optimal point, the heatsink had a mass of around 307.8 grams, and the microprocessor experienced a temperature of about 83.52 degrees Celsius.
- ✓ Moreover, before the Global Minimum point, it was found that there was sufficient space between two consecutive fins. Hence, increasing fins resulted in more surface area

without disruption of airflow. In this case, more surface area helped to dissipate more heat.

- ✓ Conversely, after reaching the Global Minimum point by gradual increment in the number of fins, the space between two consecutive fins became so narrow that airflow became downfall. So, the average heat transfer coefficient started to fall, and the microprocessor's temperature started increasing after the optimal fin number point. To put it another way, higher fin density (number of fins) increases airflow resistance after the Global Minimum point, which can limit heat dissipation. Thus, thermal resistance increases.
- ✓ Afterward, the Global Minimum turning point, the curve — microprocessor temperature vs fin numbers — of thick fins is more sloppy than thin fins when the length, width, height, and even materials are maintained constant.

The research work addresses the critical issue of reducing the required heatsink materials, which results in a lower material cost and weight of the heatsink while decreasing the temperature of the microprocessor. Since the modern world has been shifting towards miniature and lightweight computers at a minimal price; thus, the research work provides a real-life panacea to a convoluted problem by providing a solution that satisfies lightweight and better of heat transfer. By optimizing heatsink mass and performance, this study paves the way for a more reliable and energy-efficient desktop CPU, supporting the rapid growth of technology in modern computers.

4.2. Limitations and future works

Although the study has yielded important results, it has some limitations. Due to the financial constraints, no experimental validation could be carried out in this study. Moreover, to avoid the complexity of the simulation analysis, other small components such as resistors, capacitors, and transistors were excluded from the simulation model, which was a minor drawback of this research work. Hence, future studies should validate the simulation result via experimental tests. In addition, future studies should also try to optimize similar designs, incorporating the complexities related to the small electrical elements, to show a true representation of the CPUs. Another future study may be carried out in order to find out the optimized situation of a circular-type heatsink via the same method presented in this study. Furthermore, tinier fin thickness should be investigated until it can prevent the fin's shape deformation. Because minute thickness fins tend to be distorted. Additionally, instead of using commercial simulation software, mathematical models may be developed and used directly via programming languages such as Python.

Authorship Contributions

Md Nazmul Hasan Dipu worked on idea generation, manuscript writing, research method development, tool selection, CAD model development, and performed simulation analysis for 1-millimeter fin thickness.

Mahbub Hasan Apu worked on Photoshop tasks, manuscript writing, Excel graphs plotting, and performed simulation analysis for 1.5-millimeter fin thickness.

Pritidipto Paul Chowdhury worked on manuscript writing and performed simulation analysis for a 2-millimeter fin thickness.

Declaration of conflicting interests

The authors declare no competing interests.

Funding

The author received no financial support for the research and/or authorship of this article

Ethics

There are no ethical issues with the publication of this manuscript.

References

1. Khattak, Z., & Ali, H. M. (2019). Air cooled heat sink geometries subjected to forced flow: A critical review. *International Journal of Heat and Mass Transfer*, *130*, 141–161.
2. Sung, G., Kang, H.-M., & Yook, S.-J. (2025). Effect of installing rings on the cooling performance of a pin fin heatsink. *International Journal of Thermal Sciences*, *210*, 109660.
3. Liu, X., Hao, B., Xie, L., & Zhao, Y. (2025). Research and application of topology optimization on air-cooled heat sinks. *Applied Thermal Engineering*, 125607.
4. Patel, H., & Matawala, V. K. (2019). Performance evaluation and parametric optimization of a heat sink for cooling of electronic devices with entropy generation minimization. *European Journal of Sustainable Development Research*, *3*(4).
5. Armstrong, R., & Fast, D. (2004). Thermal characterization and optimization of a blower heat sink for small form factor micro-computer desktop applications. In *The Ninth Intersociety Conference on Thermal and Thermomechanical Phenomena In Electronic Systems (IEEE Cat. No.04CH37543)* (pp. 659–663). IEEE.
6. Yu, C.-W., & Webb, R. L. (2001). Thermal design of a desktop computer system using CFD analysis. In *Seventeenth Annual IEEE Semiconductor Thermal Measurement and Management Symposium (Cat. No.01CH37189)* (pp. 18–26). IEEE.
7. Heat Sinks. (2022). In *Thermal Design* (pp. 45–117). Wiley.
8. Hajialibabaei, M., Saghir, M. Z., & Bicer, Y. (2023). Comparing the performance of a straight-channel heat sink with different channel heights: an experimental and numerical study. *Energies*, *16*(9), 3825.
9. Chen, C., Huang, Z., & Li, M. (2024). Study on the effect of fin position on heat dissipation effect of finned heat sinks.
10. Jones, A., & Darabi, J. (2024). Enhancing thermal performance in a pcm heatsink assembly by incorporating fins and copper oxide nanoparticles. In *ASME 2024 Heat*

Transfer Summer Conference. American Society of Mechanical Engineers.

11. Jones, A., & Darabi, J. (2024). Effect of fin geometry on the thermal performance of a phase change material heatsink. *Applied Thermal Engineering*, *236*, 121973.
12. Vallepuga-Espinosa, J., Cifuentes-Rodríguez, J., Gutiérrez-Posada, V., & Ubero-Martínez, I. (2022). Thermomechanical optimization of three-dimensional low heat generation microelectronic packaging using the boundary element method. *Mathematics*, *10*(11), 1913.
13. Ledezma, G., & Bejan, A. (1996). Heat sinks with sloped plate fins in natural and forced convection. *International Journal of Heat and Mass Transfer*, *39*(9), 1773–1783.
14. Chang, S. W., Su, L. M., Yang, T. L., & Chiou, S. F. (2004). Enhanced heat transfer of forced convective fin flow with transverse ribs. *International Journal of Thermal Sciences*, *43*(2), 185–200.
15. Park, K., Oh, P.-K., & Lim, H.-J. (2006). The application of the CFD and Kriging method to an optimization of heat sink. *International Journal of Heat and Mass Transfer*, *49*(19–20), 3439–3447.
16. Ozturk, E., & Tari, I. (2008). Forced air cooling of cpus with heat sinks: A numerical study. *IEEE Transactions on Components and Packaging Technologies*, *31*(3), 650–660.
17. Hussain, A. A., Freegah, B., Khalaf, B. S., & Towsyfyan, H. (2019). Numerical investigation of heat transfer enhancement in plate-fin heat sinks: Effect of flow direction and fillet profile. *Case Studies in Thermal Engineering*, *13*, 100388.
18. Abdelmohimen, M. A. H., Algarni, S., Almutairi, K., Ahmed, G. M. S., Irshad, K., & Irfan, S. A. (2021). Improving heat transfer of plate-fin heat sinks using through rod configurations. *Journal of Thermal Science and Engineering Applications*, *13*(1).
19. Kalbasi, R., Afrand, M., Alsarraf, J., & Tran, M.-D. (2019). Studies on optimum fins number in PCM-based heat sinks. *Energy*, *171*, 1088–1099.
20. Mohan, R., & Govindarajan, P. (2011). Experimental and CFD analysis of heat sinks with base plate for CPU cooling. *Journal of Mechanical Science and Technology*, *25*(8), 2003–2012.
21. Chiu, H.-C., Youh, M.-J., Hsieh, R.-H., Jang, J.-H., & Kumar, B. (2023). Numerical investigation on the temperature uniformity of micro-pin-fin heat sinks with variable density arrangement. *Case Studies in Thermal Engineering*, *44*, 102853.
22. Koşar, A., & Peles, Y. (2006). Thermal-hydraulic performance of mems-based pin fin heat sink. *Journal of Heat Transfer*, *128*(2), 121–131.
23. Koşar, A., Mishra, C., & Peles, Y. (2005). Laminar flow across a bank of low aspect ratio micro pin fins. *Journal of Fluids Engineering*, *127*(3), 419–430.
24. Jassani, A. J. J. Al. (2020). Experimental study for optimum fin spacing of rectangular fin arrangements under the influences of free convection. *Journal of Engineering Science and Technology*, *15*(6), 4075–4090.
25. Wu, Q. (2020). Evaluating a multi-jet impingement air heat exchanger design for pebb 6000 using solidworks flow simulation. *Massachusetts Institute Of Technology*.
26. Micheli, L., Reddy, K. S., & Mallick, T. K. (2016). Thermal effectiveness and mass usage of horizontal micro-fins under natural convection. *Applied Thermal Engineering*, *97*, 39–47.
27. Çengel, Y. A., & Ghajar, A. J. (2015). Heat_and_mass_transfer (5th ed.).
28. Balaji, C., Srinivasan, B., & Gedupudi, S. (2021). One-dimensional, steady state heat conduction. In *Heat Transfer Engineering* (pp. 15–64).
29. Forsberg, C. H. (2021). Steady-state conduction. In *Heat Transfer Principles and Applications* (pp. 57–120).
30. Li, B., Cui, Z., Cao, Q., & Shao, W. (2021). Increasing Efficiency of a Finned Heat Sink Using Orthogonal Analysis. *Energies*, *14*(3), 782.
31. Sehnalek, S., Zalesak, M., Vincenec, J., Oplustil, M., & Chrobak, P. (2014). Evaluation of solidworks flow simulation byground-coupled heat transfer test cases. *Island Santorini: International Conferences: Latest Trends on Systems*.
32. Bistafa, S. R. (2017). On the development of the Navier-Stokes equation by Navier. *Revista Brasileira de Ensino de Física*, *40*(2).
33. Madhavan, S., P B, R. D., Gundabattini, E., & Mystkowski, A. (2022). Thermal analysis and heat management strategies for an induction motor, a review. *Energies*, *15*(21), 8127.
34. Ramakrishnan, B., Alissa, H., Manousakis, I., Lankston, R., Bianchini, R., Kim, W., … Fontoura, M. (2021). CPU overclocking: a performance assessment of air, cold plates, and two-phase immersion cooling. *IEEE Transactions on Components, Packaging and Manufacturing Technology*, *11*(10), 1703–1715.
35. Tijani, A. S., & Jaffri, N. B. (2018). Thermal analysis of perforated pin-fins heat sink under forced convection condition. *Procedia Manufacturing*, *24*, 290–298.
36. Varuvel, E. G., Sonthalia, A., Aloui, F., & Saravanan, C. G. (2023). Basics of heat transfer: convection. In *Handbook of Thermal Management Systems* (pp. 35–77). Elsevier.
37. Ökten, E., Kırcı, L., & Kılıçlı, Ö. (2022). Power and thermal analysis of a pcm-cooled photovoltaic thermal system with a 1-d mathematical model for different environmental and boundary conditions: A case study. *International Journal of Pioneering Technology and Engineering*, *2*(02), 193–201.

38. Abbas, E. F. (2024). An overview of heat sink technology. *International Journal of Applied Mechanics and Engineering*, *29*(4), 1–23.

39. Intel® Core™ i9-9900K Processor 16M Cache, up to 5.00 GHz. (2018). Retrieved 17 January 2025, from https://www.intel.com/content/www/us/en/products/sku/186605/intel-core-i99900k-processor-16m-cache-up-to-5-00-ghz/specifications.html

40. Wallossek, I. (2018). Igor's Lab. Retrieved 17 January 2025, from https://www.igorslab.de/en/intel-core-i9-9900k-i7-9700k-i5-9600k-in-test-review/13/

41. Kyono, K., Fukunaga, N., Haigo, K., Chiba, S., Nakajo, Y., & Fuchinoue, K. (2002). A constant room temperature of 25°c significantly enhances the efficacy of in-vitro fertilization. *Journal of Mammalian Ova Research*, *19*(3), 128–129.

42. Dong, D., & Lu, Y.-C. (2023). Working at room temperature. *Science*, *379*(6631), 436–437.

43. Tochihara, Y., Hashiguchi, N., Yadoguchi, I., Kaji, Y., & Shoyama, S. (2012). Effects of room temperature on physiological and subjective responses to bathing in the elderly. *Journal of the Human-Environment System*, *15*(1), 13–19.

44. Nallabelli, A., Lujan, H. L., & DiCarlo, S. E. (2024). Pressure never sucks, pressure only pushes: a physiological exploration of the pushing power of pressure. *Advances in Physiology Education*, *48*(3), 558–565.

45. Sonntag, D. (1982). New values for the thermodynamic parameters of water vapor. *Measurement Techniques*, *25*(9), 764–767.

46. Wubieneh, T. A., & Tegegne, S. T. (2022). Fabrication and characterization of aluminum (al-6061) matrix composite reinforced with waste glass for engineering applications. *Journal of Nanomaterials*, *2022*(1).

47. Senapati, A. K., Abhishek-Kumar, & Anurag-Kumar. (2018). Investigation on mechanical properties of al-6061 alloy based MMC. *IOP Conference Series: Materials Science and Engineering*, *410*, 012016.

48. *Fujipoly New Product Technical Information Sarcon GR25A Series*. (2012).

49. Sosnowski, M. (2018). Computational domain discretization in numerical analysis of flow within granular materials. *EPJ Web of Conferences*, *180*, 02095.

50. Abu-Zidan, Y., Mendis, P., & Gunawardena, T. (2021). Optimising the computational domain size in CFD simulations of tall buildings. *Heliyon*, *7*(4), e06723.

51. Azmi, M. Z., & Ito, T. (2020). Artificial potential field with discrete map transformation for feasible indoor path planning. *Applied Sciences*, *10*(24), 8987.

52. Tu, J., Yeoh, G. H., & Lui, C. (2018). Computational_fluid_dynamics: A practical approach.